Critical initialisation for deep signal propagation in noisy rectifier neural networks

Arnu Pretorius*

Computer Science Division CAIR[†] Stellenbosch University

Elan Van Biljon

Computer Science Division Stellenbosch University

Steve Kroon

Computer Science Division Stellenbosch University

Herman Kamper

Department of Electrical and Electronic Engineering Stellenbosch University

Abstract

Stochastic regularisation is an important weapon in the arsenal of a deep learning practitioner. However, despite recent theoretical advances, our understanding of how noise influences signal propagation in deep neural networks remains limited. By extending recent work based on mean field theory, we develop a new framework for signal propagation in stochastic regularised neural networks. Our noisy signal propagation theory can incorporate several common noise distributions, including additive and multiplicative Gaussian noise as well as dropout. We use this framework to investigate initialisation strategies for noisy ReLU networks. We show that no critical initialisation strategy exists using additive noise, with signal propagation exploding regardless of the selected noise distribution. For multiplicative noise (e.g. dropout), we identify alternative critical initialisation strategies that depend on the second moment of the noise distribution. Simulations and experiments on real-world data confirm that our proposed initialisation is able to stably propagate signals in deep networks, while using an initialisation disregarding noise fails to do so. Furthermore, we analyse correlation dynamics between inputs. Stronger noise regularisation is shown to reduce the depth to which discriminatory information about the inputs to a noisy ReLU network is able to propagate, even when initialised at criticality. We support our theoretical predictions for these trainable depths with simulations, as well as with experiments on MNIST and CIFAR-10.[‡]

1 Introduction

Over the last few years, advances in network design strategies have made it easier to train large networks and have helped to reduce overfitting. These advances include improved weight initialisation strategies (Glorot and Bengio, 2010; Saxe et al., 2014; Sussillo and Abbott, 2014; He et al., 2015; Mishkin and Matas, 2016), non-saturating activation functions (Glorot et al., 2011) and stochastic regularisation techniques (Srivastava et al., 2014). Authors have noted, for instance, the critical dependence of successful training on noise-based methods such as dropout (Krizhevsky et al., 2012; Dahl et al., 2013).

^{*}Correspondence: arnupretorius@gmail.com

[†]CSIR/SU Centre for Artificial Intelligence Research.

[‡]Code to reproduce all the results is available at https://github.com/ElanVB/noisy_signal_prop

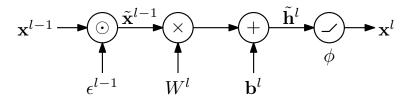


Figure 1: Noisy layer recursion. The input \mathbf{x}^{l-1} from the previous layer gets corrupted by the sampled noise ϵ^{l-1} , either by vector addition or component-wise multiplication, producing the noisy inputs $\tilde{\mathbf{x}}^{l-1}$. The l^{th} layer's corrupted pre-activations are then computed by multiplication with the layer weight matrix W^l , followed by a vector addition of the biases \mathbf{b}^l . Finally, the inputs to the next layer are simply the activations of the current layer, i.e. $\mathbf{x}^l = \phi(\tilde{\mathbf{h}}^l)$.

In many cases, successful results arise only from effective combination of these advances. Despite this interdependence, our theoretical understanding of how these mechanisms and their interactions affect neural networks remains impoverished.

One approach to studying these effects is through the lens of deep neural signal propagation. By modelling the empirical input variance dynamics at the point of random initialisation, Saxe et al. (2014) were able to derive equations capable of describing how signal propagates in nonlinear fully connected feed-forward neural networks. This "mean field" theory was subsequently extended by Poole et al. (2016) and Schoenholz et al. (2017), in particular, to analyse signal correlation dynamics. These analyses highlighted the existence of a critical boundary at initialisation, referred to as the "edge of chaos". This boundary defines a transition between ordered (vanishing), and chaotic (exploding) regimes for neural signal propagation. Subsequently, the mean field approximation to random neural networks has been employed to analyse other popular neural architectures (Yang and Schoenholz, 2017; Xiao et al., 2018; Chen et al., 2018).

This paper focuses on the effect of noise on signal propagation in deep neural networks. Firstly we ask: How is signal propagation in deep neural networks affected by noise? To gain some insight into this question, we extend the mean field theory developed by Schoenholz et al. (2017) for the special case of dropout noise, into a generalised framework capable of describing the signal propagation behaviour of stochastically regularised neural networks for different noise distributions.

Secondly we ask: How much are current weight initialisation strategies affected by noise-induced regularisation in terms of their ability to initialise at a critical point for stable signal propagation? Using our derived theory, we investigate this question specifically for rectified linear unit (ReLU) networks. In particular, we show that no such critical initialisation exists for arbitrary zero-mean additive noise distributions. However, for multiplicative noise, such an initialisation is shown to be possible, given that it takes into account the amount of noise being injected into the network. Using these insights, we derive novel critical initialisation strategies for several different multiplicative noise distributions.

Finally, we ask: Given that a network is initialised at criticality, in what way does noise influence the network's ability to propagate useful information about its inputs? By analysing the correlation between inputs as a function of depth in random deep ReLU networks, we highlight the following: even though the statistics of individual inputs are able to propagate arbitrarily deep at criticality, *discriminatory information* about the inputs becomes lost at shallower depths as the noise in the network is increased. This is because in the later layers of a random noisy network, the internal representations from different inputs become uniformly correlated. Therefore, the application of noise regularisation directly limits the trainable depth of critically initialised ReLU networks.

2 Noisy signal propagation

We begin by presenting mean field equations for stochastically regularised fully connected feed-forward neural networks, allowing us to study noisy signal propagation for a variety of noise distributions. To understand how noise influences signal propagation in a random network given an input $\mathbf{x}^0 \in \mathbb{R}^{D_0}$, we inject noise into the model

$$\tilde{\mathbf{h}}^l = W^l(\mathbf{x}^{l-1} \odot \epsilon^{l-1}) + \mathbf{b}^l, \quad \text{for } l = 1, ..., L$$
 (1)

using the operator \odot to denote either addition or multiplication where ϵ^l is an input noise vector, sampled from a pre-specified noise distribution. For additive noise, the distribution is assumed to be zero mean, for multiplicative noise distributions, the mean is assumed to be equal to one. The weights $W^l \in \mathbb{R}^{D_l \times D_{l-1}}$ and biases $\mathbf{b}^l \in \mathbb{R}^{D_l}$ are sampled i.i.d. from zero mean Gaussian distributions with variances σ_w^2/D_{l-1} and σ_b^2 , respectively, where D_l denotes the dimensionality of the l^{th} hidden layer in the network. The hidden layer activations $\mathbf{x}^l = \phi(\tilde{\mathbf{h}}^l)$ are computed element-wise using an activation function $\phi(\cdot)$, for layers l=1,...,L. Figure 1 illustrates this recursive sequence of operations.

To describe forward signal propagation for the model in (1), we make use of the mean field approximation as in Poole et al. (2016) and analyse the statistics of the internal representations of the network in expectation over the parameters and the noise. Since the weights and biases are sampled from zero mean Gaussian distributions with pre-specified variances, we can approximate the distribution of the pre-activations at layer l, in the large width limit, by a zero mean Gaussian with variance

$$\tilde{q}^{l} = \sigma_w^2 \left\{ \mathbb{E}_z \left[\phi \left(\sqrt{\tilde{q}^{l-1}} z \right)^2 \right] \odot \mu_2^{l-1} \right\} + \sigma_b^2, \tag{2}$$

where $z \sim \mathcal{N}(0,1)$ (see Section A.1 in the supplementary material). Here, $\mu_2^l = \mathbb{E}_{\epsilon}[(\epsilon^l)^2]$ is the second moment of the noise distribution being sampled from at layer l. The initial input variance is given by $q^0 = \frac{1}{D_0}\mathbf{x}^0 \cdot \mathbf{x}^0$. Furthermore, to study the behaviour of a pair of signals from two different inputs, $\mathbf{x}^{0,a}$ and $\mathbf{x}^{0,b}$, passing through the network, we can compute the covariance at each layer as

$$\tilde{q}_{ab}^l = \sigma_w^2 \mathbb{E}_{z_1} \left[\mathbb{E}_{z_2} \left[\phi(\tilde{u}_1) \phi(\tilde{u}_2) \right] \right] + \sigma_b^2 \tag{3}$$

where $\tilde{u}_1 = \sqrt{\tilde{q}_{aa}^{l-1}}z_1$ and $\tilde{u}_2 = \sqrt{\tilde{q}_{bb}^{l-1}}\left[\tilde{c}^{l-1}z_1 + \sqrt{1-(\tilde{c}^{l-1})^2}z_2\right]$, with the correlation between inputs at layer l given by $\tilde{c}^l = \tilde{q}_{ab}^l/\sqrt{\tilde{q}_{aa}^l\tilde{q}_{bb}^l}$. Here, q_{aa}^l is the variance of $\tilde{\mathbf{h}}_j^{l,a}$ (see Section A.2 in the supplementary material for more details).

For the backward pass, we use the equations derived in Schoenholz et al. (2017) to describe error signal propagation. In the context of mean field theory, the expected magnitude of the gradient at each layer can be shown to be proportional to the variance of the error, $\tilde{\delta}_i^l = \phi'(\tilde{\mathbf{h}}_i^l) \sum_{j=1}^{D_{l+1}} \tilde{\delta}_j^{l+1} W_{ji}^{l+1}$. This allows for the distribution of the error signal at layer l to be approximated by a zero mean Gaussian with variance

$$\tilde{q}_{\delta}^{l} = \tilde{q}_{\delta}^{l+1} \frac{D_{l+1}}{D_{l}} \sigma_{w}^{2} \mathbb{E}_{z} \left[\phi' \left(\sqrt{\tilde{q}^{l}} z \right)^{2} \right]. \tag{4}$$

Similarly, for noise regularised networks, the covariance between error signals can be shown to be

$$\tilde{q}_{ab,\delta}^{l} = \tilde{q}_{ab,\delta}^{l+1} \frac{D_{l+1}}{D_{l+2}} \sigma_{w}^{2} \mathbb{E}_{z_{1}} \left[\mathbb{E}_{z_{2}} \left[\phi'(\tilde{u}_{1}) \phi'(\tilde{u}_{2}) \right] \right], \tag{5}$$

where \tilde{u}_1 and \tilde{u}_2 are defined as was done in the forward pass.

Equations (2)-(5) fully capture the relevant statistics that govern signal propagation for a random network during both the forward and the backward pass. In the remainder of this paper, we consider, as was done by Schoenholz et al. (2017), the following necessary condition for training: "for a random network to be trained information about the inputs should be able to propagate forward through the network, and information about the gradients should be able to propagate backwards through the network." The behaviour of the network at this stage depends on the choice of activation, noise regulariser and initial parameters. In the following section, we will focus on networks that use the Rectified Linear Unit (ReLU) as activation function. The chosen noise regulariser is considered a design choice left to the practitioner. Therefore, whether a random noisy ReLU network satisfies the above stated necessary condition for training largely depends on the starting parameter values of the network, *i.e.* its initialisation.

¹It is, however, important to note that the derivation relies on the assumption that the weights used in the forward pass are sampled independently from those used during backpropagation.

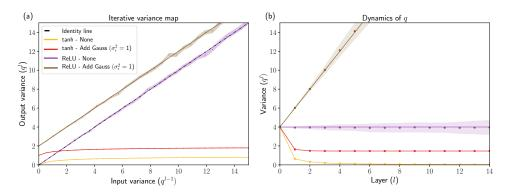


Figure 2: Deep signal propagation with and without noise. (a): Iterative variance map. (b): Variance dynamics during forward signal propagation. In (a) and (b), lines correspond to theoretical predictions and points to numerical simulations (means over 50 runs with shaded one standard deviation bounds), for noiseless tanh (yellow) and noiseless ReLU (purple) networks, as well as for noisy tanh (red) and noisy ReLU (brown) networks regularised using additive noise from a standard Gaussian. Both tanh networks use $(\sigma_w, \sigma_b) = (1,0)$, the "Xavier" initialisation (Glorot and Bengio, 2010), while the ReLU networks use $(\sigma_w, \sigma_b) = (\sqrt{2}, 0)$ the "He" initialisation (He et al., 2015). In our experiments, we use network layers consisting of 1000 hidden units (see Section C in the supplementary material for more details on all our simulated experiments).

3 Critical initialisation for noisy rectifier networks

Unlike the tanh nonlinearity investigated in previous work (Poole et al., 2016; Schoenholz et al., 2017), rectifying activation functions such as ReLU are unbounded. This means that the statistics of signal propagation through the network is not guaranteed to naturally stabilise through saturating activations, as shown in Figure 2.

A point on the identity line in Figure 2 (a) represents a fixed point to the recursive variance map in equation (2). At a fixed point, signal will stably propagate through the remaining layers of the network. For tanh networks, such a fixed point always exists irrespective of the initialisation, or the amount of noise injected into the network. For ReLU networks, this is not the case. Consider the "He" initialisation (He et al., 2015) for ReLU, commonly used in practice. In (b), we plot the variance dynamics for this initialisation in purple and observe stable behaviour. But what happens when we inject noise into each network? In the case of tanh (shown in red), the added noise simply shifts the fixed point to a new stable value. However, for ReLU, the noise entirely destroys the fixed point for the "He" initialisation, making signal propagation unstable. This can be seen in (a), where the variance map for noisy ReLU (shown in brown) moves off the identity line entirely, causing the signal in (b) to explode.

Therefore, to investigate whether signal can stably propagate through a random *noisy* ReLU network, we examine (2) more closely, which for ReLU becomes (see Section B.1 in supplementary material)

$$\tilde{q}^l = \sigma_w^2 \left[\frac{\tilde{q}^{l-1}}{2} \odot \mu_2 \right] + \sigma_b^2. \tag{6}$$

For ease of exposition we assume equal noise levels at each layer, i.e. $\mu_2^l = \mu_2, \forall l$. A critical initialisation for a noisy ReLU network occurs when the tuple $(\sigma_w, \sigma_b, \mu_2)$ provides a fixed point \tilde{q}^* , to the recurrence in (6). This at least ensures that the statistics of individual inputs to the network will be preserved throughout the first forward pass. The existence of such a solution depends on the type of noise that is injected into the network. In the case of additive noise, $\tilde{q}^* = \sigma_w^2 \frac{1}{2} \tilde{q}^* + \mu_2 \sigma_w^2 + \sigma_b^2$, implying that the only critical point initialisation for non-zero \tilde{q}^* is given by $(\sigma_w, \sigma_b, \mu_2) = (\sqrt{2}, 0, 0)$. Therefore, critical initialisation is not possible using any amount of zero-mean additive noise, regardless of the noise distribution. For multiplicative noise, $\tilde{q}^* = \sigma_w^2 \frac{1}{2} \tilde{q}^* \mu_2 + \sigma_b^2$, so the solution $(\sigma_w, \sigma_b, \mu_2) = \left(\sqrt{\frac{2}{\mu_2}}, 0, \mu_2\right)$ provides a critical initialisation for noise distributions with mean one and a non-zero second moment μ_2 . For example, in the case of multiplicative Gaussian noise, $\mu_2 = \sigma_\epsilon^2 + 1$, yielding critical initialisation with $(\sigma_w, \sigma_b) = \left(\sqrt{\frac{2}{\sigma^2+1}}, 0\right)$. For dropout noise,

Table 1: Critical point initialisation for noisy ReLU networks.

DISTRIBUTION	$P(\epsilon)$	μ_2	CRITICAL INITIALISATION
— Additive Noise —			
GAUSSIAN	$\mathcal{N}(0,\sigma_{\epsilon}^2)$	σ_{ϵ}^2	$(\sigma_w, \sigma_b, \sigma_\epsilon) = (\sqrt{2}, 0, 0)$
LAPLACE	$Lap(0,\beta)$	$2\beta^2$	$(\sigma_w, \sigma_b, \beta) = (\sqrt{2}, 0, 0)$
— MULTIPLICATIVE NOISE —			
Gaussian	$\mathcal{N}(1,\sigma_{\epsilon}^2)$	$(\sigma_{\epsilon}^2 + 1)$	$(\sigma_w, \sigma_b, \sigma_\epsilon) = \left(\sqrt{rac{2}{\sigma_\epsilon^2 + 1}}, 0, \sigma_\epsilon ight)$
LAPLACE	$Lap(1, \beta)$	$(2\beta^2 + 1)$	$(\sigma_w, \sigma_b, \beta) = \left(\sqrt{\frac{2}{2\beta^2 + 1}}, 0, \beta\right)$
Poisson	Poi(1)	2	$(\sigma_w, \sigma_b, \lambda) = (1, 0, 1)$
DROPOUT	$\begin{aligned} \mathbf{P}(\epsilon &= \frac{1}{p}) = p, \\ \mathbf{P}(\epsilon &= 0) &= 1 - p \end{aligned}$	$\frac{1}{p}$	$(\sigma_w, \sigma_b, p) = (\sqrt{2p}, 0, p)$

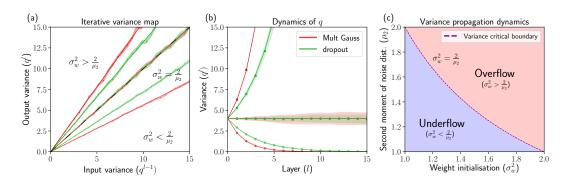


Figure 3: Critical initialisation for noisy ReLU networks. (a): Iterative variance map. (b): Variance dynamics during forward signal propagation. In (a) and (b), lines correspond to theoretical predictions and points to numerical simulations. Dropout (p=0.6) is shown in green for different initialisations, $\sigma_w^2 = 2(0.6) = \frac{2}{\mu_2}$ (critical), $\sigma_w^2 = (1.15)^2 \frac{2}{(0.6)^{-1}} > \frac{2}{\mu_2}$ (exploding signal) and $\sigma_w^2 = (0.85)^2 \frac{2}{(0.6)^{-1}} < \frac{2}{\mu_2}$ (vanishing signal). Similarly, multiplicative Gaussian noise $(\sigma_\epsilon = 0.25)$ is shown in red with $\sigma_w^2 = \frac{2}{(0.25)^2 + 1} = \frac{2}{\mu_2}$ (critical), $\sigma_w^2 = (1.25)^2 \frac{2}{\mu_2}$ (exploding) and $\sigma_w^2 = (0.75)^2 \frac{2}{\mu_2}$ (vanishing). (c): Variance critical boundary for initialisation, separating numerical overflow and underflow signal propagation regimes.

 $\mu_2=1/p$ (with p the probability of retaining a neuron); thus, to initialise at criticality, we must set $(\sigma_w,\sigma_b)=(\sqrt{2p},0)$. Table 1 summarises critical initialisations for some commonly used noise distributions. We also note that similar results can be derived for other rectifying activation functions; for example, for multiplicative noise the critical initialisation for parametric ReLU (PReLU) activations (with slope parameter α) is given by $(\sigma_w,\sigma_b,\mu_2)=\left(\sqrt{\frac{2}{\mu_2(\alpha^2+1)}},0,\mu_2\right)$.

To see the effect of initialising on or off the critical point for ReLU networks, Figure 3 compares the predicted versus simulated variance dynamics for different initialisation schemes. For schemes not initialising at criticality, the variance map in (a) no longer lies on the identity line and as a result the forward propagating signal in (b) either explodes, or vanishes. In contrast, the initialisations derived above lie on the critical boundary between these two extremes, as shown in (c) as a function of the noise. By compensating for the amount of injected noise, the signal corresponding to the initialisation $\sigma_w^2 = \frac{2}{\mu_2}$ is preserved in (b) throughout the entire forward pass, with roughly constant variance dynamics.

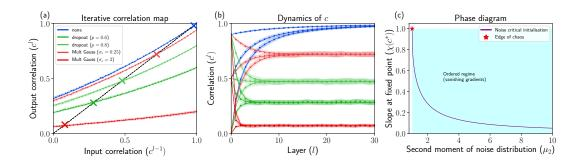


Figure 4: *Propagating correlation information in noisy ReLU networks.* (a): Iterative correlation map with fixed points indicated by "X" marks on the identity line. (b): Correlation dynamics during forward signal propagation. In (a) and (b), lines correspond to theoretical predictions and points to numerical simulations. All simulated networks were initialised at criticality for each noise type and level. (c): Slope at the fixed point correlation as a function of the amount of noise injected into the network.

Next, we investigate the correlation dynamics between inputs. Assuming that (6) is at its fixed point \tilde{q}^* , which exists only if $\sigma_w^2 = \frac{2}{\mu_2}$, the correlation map for a noisy ReLU network is given by (see Section B.2 in supplementary material)

$$\tilde{c}^{l} = \frac{1}{\mu_{2}} \left\{ \frac{\tilde{c}^{l-1} \sin^{-1} \left(\tilde{c}^{l-1} \right) + \sqrt{1 - (\tilde{c}^{l-1})^{2}}}{\pi} + \frac{\tilde{c}^{l-1}}{2} \right\}. \tag{7}$$

Figure 4 plots this theoretical correlation map against simulated dynamics for different noise types and levels. For no noise, the fixed point c^* in (a) is situated at one (marked with an "X" on the blue line). The slope of the blue line indicates a non-decreasing function of the input correlations. After a certain depth, inputs end up perfectly correlated irrespective of their starting correlation, as shown in (b). In other words, random deep ReLU networks lose discriminatory information about their inputs as the depth of the network increases, even when initialised at criticality. When noise is added to the network, inputs decorrelate and c^* moves away from one. However, more importantly, correlation information in the inputs become lost at shallower depths as the noise level increases, as can be seen in (b)

How quickly a random network loses information about its inputs depends on the rate of convergence to the fixed point c^* . Using this observation, Schoenholz et al. (2017) derived so-called depth scales ξ_c , by assuming $|c^l - c^*| \sim e^{-l/\xi_c}$. These scales essentially control the feasible depth at which networks can be considered trainable, since they may still allow useful correlation information to propagate through the network. In our case, the depth scale for a noisy ReLU network under this assumption can be shown to be (see Section B.3 in supplementary material)

$$\xi_c = -1/\ln\left[\chi(c^*)\right],\tag{8}$$

where

$$\chi(c^*) = \frac{1}{\mu_2 \pi} \left[\sin^{-1} \left(c^* \right) + \frac{\pi}{2} \right]. \tag{9}$$

The exponential rate assumption underlying the derivation of (8) is supported in Figure 5, where for different noise types and levels, we plot $|c^l - c^*|$ as a function of depth on a log-scale, with corresponding linear fits (see panels (a) and (c)). We then compare the theoretical depth scales from (8) to actual depth scales obtained through simulation (panels (b) and (d)), as a function of noise and observe a good fit for non-zero noise levels. We thus find that noise limits the depth at which critically initialised ReLU networks are expected to perform well through training.

 $^{^4}$ We note Hayou et al. (2018) recently showed that the rate of convergence for noiseless ReLU networks is not exponential, but polynomial instead. Interestingly, keeping with the exponential rate assumption, we indeed find that the discrepancy between our theoretical depth scales from (8) and our simulated depth scales, is largest at very low noise levels. However, at more typical noise levels, such as a dropout rate of p=0.5 for example, the assumption seems to provide a close fit, with good agreement between theory and simulation.

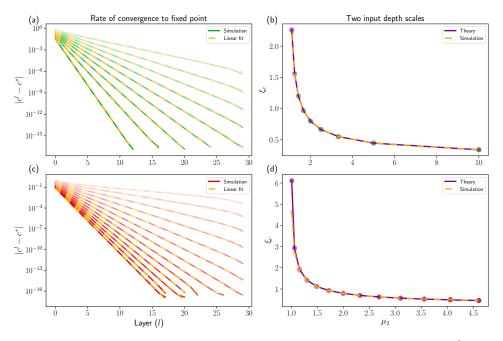


Figure 5: Noise dependent depth scales for training. (a): Linear fits (dashed lines) to $|c^l-c^*|$ as a function of depth on a log-scale (solid lines) for varying amounts of dropout (p=0.1 to p=0.9 by 0.1). (b): Theoretical depth scales (solid lines) versus empirically inferred scales (dashed lines) per dropout rate. Scales are inferred noting that if $|c^l-c^*|\sim e^{-l/\xi_c}$, then a linear fit, al+b, in the logarithmic domain gives $\xi_c\approx -\frac{1}{a}$, for large l. In other words, the negative inverse slope of a linear fit to the log differences in correlation should match the theoretical values for ξ_c . Therefore, we compare $\xi_c=-1/\ln\left[\chi(c^*)\right]$ to $-\frac{1}{a}$ for different levels of noise. (c) - (d): Similar to (a) and (b), but for Gaussian noise $(\sigma_\epsilon=0.1 \text{ to } \sigma_\epsilon=1.9 \text{ by } 0.15)$.

We next briefly discuss error signal propagation during the backward pass for noise regularised ReLU networks. When critically initialised, the error variance recurrence relation in (4) for these networks is (see Section B.4 in supplementary material)

$$\tilde{q}_{\delta}^{l} = \tilde{q}_{\delta}^{l+1} \frac{D_{l+1}}{D_{l}\mu_{2}},\tag{10}$$

with the covariance between error signals in (5), given by (see Section B.5 in supplementary material)

$$\tilde{q}_{ab,\delta}^{l} = \tilde{q}_{ab,\delta}^{l+1} \frac{D_{l+1}}{D_{l+2}} \chi(c^*). \tag{11}$$

Note the explicit dependence on the width of the layers of the network in (10) and (11). We first consider constant width networks, where $D_{l+1} = D_l$, for all l = 1, ..., L. For any amount of multiplicative noise, $\mu_2 > 1$, and we see from (10) that gradients will tend to vanish for large depths. Furthermore, Figure 4 (c) plots $\chi(c^*)$ as a function of μ_2 . As μ_2 increases from one, $\chi(c^*)$ decreases from one. Therefore, from (11), we also find that error signals from different inputs will tend to decorrelate at large depths.

Interestingly, for non-constant width networks, stable gradient information propagation may still be possible. If the network architecture adapts to the amount of noise being injected by having the widths of the layers grow as $D_{l+1} = D_l \mu_2$, then (10) should be at its fixed point solution. For example, in the case of dropout $D_{l+1} = D_l/p$, which implies that for any p < 1, each successive layer in the network needs to grow in width by a factor of 1/p to promote stable gradient flow. Similarly, for multiplicative Gaussian noise, $D_{l+1} = D_l(\sigma_\epsilon^2 + 1)$, which requires the network to grow in width unless $\sigma_\epsilon^2 = 0$. Similarly, if $D_{l+2} = D_{l+1}\chi(c^*) = D_l\mu_2\chi(c^*)$ in (11), the covariance of the error signal should be preserved during the backward pass, for arbitrary values of μ_2 and $\chi(c^*)$.

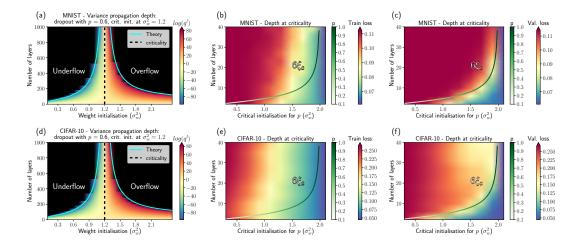


Figure 6: Depth scale experiments on MNIST and CIFAR-10. (a) Variance propagation dynamics for MNIST on and off the critical point initialisation (dashed black line) with dropout (p=0.6). The cyan curve represents the theoretical boundary at which numerical instability issues are predicted to occur and is computed as $L^* = \ln(K)/\ln(\frac{\sigma_w^2}{2}\mu_2)$, where K is the largest (or smallest) positive number representable by the computer. Specifically, we use 32-bit floating point numbers and set $K=3.4028235\times 10^{38}$, if $\sigma_w^2>\frac{2}{\mu_2}$ and $K=1.1754944\times 10^{-38}$, if $\sigma_w^2<\frac{2}{\mu_2}$. (b) Depth scales fit to the training loss on MNIST for networks initialised at criticality for dropout rates p=0.1 (severe dropout) to p=1 (no dropout). (c) Depth scales fit to the validation loss on MNIST. (d) - (f): Similar to (a) - (c), but for CIFAR-10. For each plot we highlight trends by smoothing the colour grid (for non smoothed versions see Section C.5 in the supplementary material).

4 Experimental results

From our analysis of deep noisy ReLU networks in the previous section, we expect that a necessary condition for such a network to be trainable, is that the network be initialised at criticality. However, whether the layer widths are varied or not for the sake of backpropagation, the correlation dynamics in the forward pass may still limit the depth at which these networks perform well.

We therefore investigate the performance of noise-regularised deep ReLU networks on real-world data. First, we validate the derived critical initialisation. As the depth of the network increases, any initialisation strategy that does not factor in the effects of noise, will cause the forward propagating signal to become increasingly unstable. For very deep networks, this might cause the signal to either explode or vanish, even within the first forward pass, making the network untrainable. To test this, we sent inputs from MNIST and CIFAR-10 through ReLU networks using dropout (with p=0.6) at varying depths and for different initialisations of the network. Figure 6 (a) and (d) shows the evolution of the input statistics as the input propagates through each network for the different data sets. For initialisations not at criticality, the variance grows or shrinks rapidly to the point of causing numerical overflow or underflow (indicated by black regions). For deep networks, this can happen well before any signal is able to reach the output layer. In contrast, initialising at criticality (as shown by the dashed black line), allows for the signal to propagate reliably even at very large depths. Furthermore, given the floating point precision, if $\sigma_w^2 \neq \frac{2}{\mu_2}$, we can predict the depth at which numerical overflow

(or underflow) will occur by solving for L^* in $K = \left(\sigma_w^2 \mu_2/2\right)^{L^*} q^0$, where K is the largest (or smallest) positive number representable by the computer (see Section C.4 in supplementary material). These predictions are shown by the cyan line and provide a good fit to the empirical limiting depth from numerical instability.

We now turn to the issue of limited trainability. Due to the loss of correlation information between inputs as a function of noise and network depth, we expect noisy ReLU networks not to be able to perform well beyond certain depths. We investigated depth scales for ReLU networks with dropout initialised at criticality: we trained 100 networks on MNIST and CIFAR-10 for 200 epochs using SGD and a learning rate of 10^{-3} with dropout rates ranging from 0.1 to 1 for varying depths. The results

are shown in Figure 6 (see Section C.5 of the supplementary material for additional experimental results). For each network configuration and noise level, the critical initialisation $\sigma_w^2 = \frac{2}{\mu_2}$ was used. We indeed observe a relationship between depth and noise on the loss of a network, even at criticality. Interestingly, the line $6\xi_c$ (Schoenholz et al., 2017), seems to track the depth beyond which the relative performance on the validation loss becomes poor, more so than on the training loss. However, in both cases, we find that even modest amounts of noise can limit performance.

5 Discussion

By developing a general framework to study signal propagation in noisy neural networks, we were able to show how different stochastic regularisation strategies may impact the flow of information in a deep network. Focusing specifically on ReLU networks, we derived novel critical initialisation strategies for multiplicative noise distributions and showed that no such critical initialisations exist for commonly used additive noise distributions. At criticality however, our theory predicts that the statistics of the input should remain within a stable range during the forward pass and enable reliable signal propagation for noise regularised deep ReLU networks. We verified these predictions by comparing them with numerical simulations as well as experiments on MNIST and CIFAR-10 using dropout and found good agreement.

Interestingly, we note that a dropout rate of p=0.5 has often been found to work well for ReLU networks (Srivastava et al., 2014). The critical initialisation corresponding to this rate is $(\sigma_w, \sigma_b) = (\sqrt{2p}, 0) = (1, 0)$. This is exactly the "Xavier" initialisation proposed by Glorot and Bengio (2010), which prior to the development of the "He" initialisation, was often used in combination with dropout (Simonyan and Zisserman, 2014). This could therefore help to explain the initial success associated with this specific dropout rate. Similarly, Srivastava et al. (2014) reported that adding multiplicative Gaussian noise where $\epsilon \sim \mathcal{N}(1, \sigma_\epsilon^2)$, with $\sigma_\epsilon^2 = 1$, also seemed to perform well, for which the critical initialisation is $\left(\sqrt{\frac{2}{\sigma_\epsilon^2+1}},0\right) = (1,0)$, again corresponding to the "Xavier" method.

Although our initialisations ensure that individual input statistics are preserved, we further analysed the correlation dynamics between inputs and found the following: at large depths inputs become predictably correlated with each other based on the amount of noise injected into the network. As a consequence, the representations for different inputs to a deep network may become indistinguishable from each other in the later layers of the network. This can make training infeasible for noisy ReLU networks of a certain depth and depends on the amount of noise regularisation being applied.

We now note the following shortcomings of our work: firstly, our findings only apply to fully connected feed-forward neural networks and focus almost exclusively on the ReLU activation function. Furthermore, we limit the scope of our architectural design to a recursive application of a dense layer followed by a noise layer, whereas in practice a larger mix of layers is usually required to solve a specific task.

Ultimately, we are interested in reducing the number of decisions that need to made when designing deep neural networks and understanding the implications of those decisions on network behaviour and performance. Any machine learning engineer exploring a neural network based solution to a practical problem will be faced with a large number of possible design decisions. All these decisions cost valuable time to explore. In this work, we hope to have at least provided some guidance in this regard, specifically when choosing between different initialisation strategies for noise regularised ReLU networks and understanding their associated implications.

Acknowledgements

We would like to thank the reviewers for their insightful comments which improved the quality of this work. Furthermore, we would like to thank Google, the CSIR/SU Centre for Artificial Intelligence Research (CAIR) as well as the Science Faculty and the Postgraduate and International Office of Stellenbosch University for financial support. Finally, we gratefully acknowledge the support of NVIDIA Corporation with the donation of a Titan Xp GPU used for this research.

References

- X. Glorot and Y. Bengio, "Understanding the difficulty of training deep feedforward neural networks," in *Proceedings of the International Conference on Artificial Intelligence and Statistics*, 2010, pp. 249–256.
- A. M. Saxe, J. L. McClelland, and S. Ganguli, "Exact solutions to the nonlinear dynamics of learning in deep linear neural networks," *Proceedings of the International Conference on Learning Representations*, 2014.
- D. Sussillo and L. Abbott, "Random walk initialization for training very deep feedforward networks," *arXiv preprint arXiv:1412.6558*, 2014.
- K. He, X. Zhang, S. Ren, and J. Sun, "Delving deep into rectifiers: Surpassing human-level performance on ImageNet classification," in *Proceedings of the IEEE International Conference on Computer Vision*, 2015, pp. 1026–1034.
- D. Mishkin and J. Matas, "All you need is a good init," *Proceedings of International Conference on Learning Representations*, 2016.
- X. Glorot, A. Bordes, and Y. Bengio, "Deep sparse rectifier neural networks," in *Proceedings of the International Conference on Artificial Intelligence and Statistics*, 2011, pp. 315–323.
- N. Srivastava, G. E. Hinton, A. Krizhevsky, I. Sutskever, and R. Salakhutdinov, "Dropout: a simple way to prevent neural networks from overfitting." *Journal of Machine Learning Research*, vol. 15, no. 1, pp. 1929–1958, 2014.
- A. Krizhevsky, I. Sutskever, and G. E. Hinton, "ImageNet classification with deep convolutional neural networks," in *Advances in Neural Information Processing Systems*, 2012, pp. 1097–1105.
- G. E. Dahl, T. N. Sainath, and G. E. Hinton, "Improving deep neural networks for LVCSR using rectified linear units and dropout," in *Proceedings of the IEEE International Conference on Acoustics, Speech and Signal Processing*, 2013, pp. 8609–8613.
- B. Poole, S. Lahiri, M. Raghu, J. Sohl-Dickstein, and S. Ganguli, "Exponential expressivity in deep neural networks through transient chaos," in *Advances in Neural Information Processing Systems*, 2016, pp. 3360–3368.
- S. S. Schoenholz, J. Gilmer, S. Ganguli, and J. Sohl-Dickstein, "Deep information propagation," *Proceedings of the International Conference on Learning Representations*, 2017.
- G. Yang and S. Schoenholz, "Mean field residual networks: On the edge of chaos," in *Advances in Neural Information Processing Systems*, 2017, pp. 7103–7114.
- L. Xiao, Y. Bahri, J. Sohl-Dickstein, S. S. Schoenholz, and J. Pennington, "Dynamical isometry and a mean field theory of CNNs: How to train 10,000-layer vanilla convolutional neural networks," *Proceedings of the International Conference on Machine Learning*, 2018.
- M. Chen, J. Pennington, and S. S. Schoenholz, "Dynamical isometry and a mean field theory of RNNs: Gating enables signal propagation in recurrent neural networks," *Proceedings of the International Conference on Machine Learning*, 2018.
- S. Hayou, A. Doucet, and J. Rousseau, "On the selection of initialization and activation function for deep neural networks," *arXiv* preprint arXiv:1805.08266, 2018.
- K. Simonyan and A. Zisserman, "Very deep convolutional networks for large-scale image recognition," arXiv preprint arXiv:1409.1556, 2014.

Supplementary Material

In this section, we provide additional details of derivations and experimental results presented in the paper.

A Signal propagation in noise regularised neural networks

To review, given an input $\mathbf{x}^0 \in \mathbb{R}^{D_0}$, we consider the following noisy random network model

$$\tilde{\mathbf{h}}^{l} = W^{l}(\mathbf{x}^{l-1} \odot \epsilon^{l-1}) + \mathbf{b}^{l}, \quad \text{for } l = 1, ..., L$$
(12)

where we inject noise into the model using the operator \odot to denote either addition or multiplication. The vector ϵ^l is an input noise vector, sampled from a pre-specified noise distribution. For additive noise, the distribution is assumed to be zero mean. Whereas for multiplicative noise distributions, the mean is assumed to be equal to one. The weights $W^l \in \mathbb{R}^{D_l \times D_{l-1}}$ and biases $\mathbf{b}^l \in \mathbb{R}^{D_l}$ are sampled i.i.d. from zero mean Gaussian distributions with variances σ_w^2/D_{l-1} and σ_b^2 , respectively, where D_l denotes the dimensionality of the l^{th} hidden layer in the network. The hidden layer activations $\mathbf{x}^l = \phi(\tilde{\mathbf{h}}^l)$ are computed element-wise using an activation function $\phi(\cdot)$, for layers l=1,...,L.

A.1 Single input signal propagation

We consider the network's behavior at initialisation. In this setting, the expected mean (over the weights, biases and noise distribution) of a unit in the pre-activations $\tilde{\mathbf{h}}_{j}^{l}$ for a single signal passing through the network will be zero with variance

$$\begin{split} \tilde{q}^l &= \mathbb{E}_{\mathbf{w}, \mathbf{b}, \epsilon}[(\tilde{\mathbf{h}}_j^l)^2] \\ &= \mathbb{E}_{\mathbf{w}, \epsilon}[\{\mathbf{w}^{l,j} \cdot (\mathbf{x}_j^{l-1} \odot \epsilon_j^{l-1})\}^2] + \mathbb{E}_{\mathbf{b}}[(\mathbf{b}_j^l)^2] \\ &= \sigma_w^2 \frac{1}{D_{l-1}} \sum_{j=1}^{D_{l-1}} \left[\phi(\tilde{\mathbf{h}}_j^{l-1})^2 \odot \mathbb{E}_{\epsilon}[(\epsilon_j^{l-1})^2] \right] + \sigma_b^2 \ , \end{split}$$

where we use $\mathbf{w}^{l,j}$ to denote the j-th row of W^l . The second last line relies on the bias distribution being zero mean, while the final step makes use of the independence between the inputs and the noise in the multiplicative case, and the noise being zero mean in the additive case. Furthermore, to ensure the expected value of the pre-activations remain unbiased, we only consider additive noise distributions with zero mean and multiplicative noise distributions with a mean equal to one. As in Poole et al. (2016), we make the self averaging assumption and consider the large layer width case where the previous layer's pre-activations are assumed to be Gaussian with zero mean and variance \tilde{q}^{l-1} . This gives the following noisy variance map

$$\tilde{q}^{l} = \sigma_w^2 \left\{ \mathbb{E}_z \left[\phi \left(\sqrt{\tilde{q}^{l-1}} z \right)^2 \right] \odot \mu_2^{l-1} \right\} + \sigma_b^2, \tag{13}$$

where $z \sim \mathcal{N}(0,1)$ and $\mu_2^l = \mathbb{E}_{\epsilon}[(\epsilon^l)^2]$ is the second moment of the noise distribution being sampled from at layer l. The initial input variance is given by $q^0 = \frac{1}{D_0}\mathbf{x}^0 \cdot \mathbf{x}^0$.

A.2 Two input signal propagation

To study the behaviour of a pair of signals, $\mathbf{x}^{0,a}$ and $\mathbf{x}^{0,b}$, passing through the network, we can compute the covariance in expectation over the noise and the parameters as

$$\begin{split} \tilde{q}_{ab}^{l} &= \mathbb{E}_{\mathbf{w},\mathbf{b},\epsilon} \big[\tilde{\mathbf{h}}_{j}^{l,a} \tilde{\mathbf{h}}_{j}^{l,b} \big] \\ &= \mathbb{E}_{\mathbf{w},\mathbf{b},\epsilon} \left[\left(\mathbf{w}^{l,j} \cdot (\mathbf{x}_{j}^{l-1,a} \odot \epsilon_{j}^{l-1,a}) + \mathbf{b}_{j}^{l} \right) \left(\mathbf{w}^{l,j} \cdot (\mathbf{x}_{j}^{l-1,b} \odot \epsilon_{j}^{l-1,b}) + \mathbf{b}_{j}^{l} \right) \right] \\ &= \mathbb{E}_{\mathbf{w},\mathbf{b},\epsilon} \left[\left(\mathbf{w}^{l,j} \cdot (\mathbf{x}_{j}^{l-1,a} \odot \epsilon_{j}^{l-1,a}) \right) \left(\mathbf{w}^{l,j} \cdot (\mathbf{x}_{j}^{l-1,b} \odot \epsilon_{j}^{l-1,b}) \right) \right] \\ &+ \mathbb{E}_{\mathbf{w},\mathbf{b},\epsilon} \left[\left(\mathbf{w}^{l,j} \cdot (\mathbf{x}_{j}^{l-1,a} \odot \epsilon_{j}^{l-1,a}) \right) \mathbf{b}_{j}^{l} \right] \\ &+ \mathbb{E}_{\mathbf{w},\mathbf{b},\epsilon} \left[\left(\mathbf{w}^{l,j} \cdot (\mathbf{x}_{j}^{l-1,b} \odot \epsilon_{j}^{l-1,b}) \right) \mathbf{b}_{j}^{l} \right] \\ &+ \mathbb{E}_{\mathbf{w},\mathbf{b},\epsilon} \left[\left(\mathbf{b}_{j}^{l} \right)^{2} \right]. \end{split}$$

Since the noise is i.i.d and we have that $\mathbb{E}_{\mathbf{b}}[\mathbf{b}_i^l] = 0$, we find that

$$\tilde{q}_{ab}^{l} = \mathbb{E}_{\mathbf{w}} \left[\left(\mathbf{w}^{l,j} \cdot \mathbf{x}_{j}^{l-1,a} \right) \left(\mathbf{w}^{l,j} \cdot \mathbf{x}_{j}^{l-1,b} \right) \right] + \mathbb{E}_{\mathbf{b}} \left[(\mathbf{b}_{j}^{l})^{2} \right]$$
(14)

$$= \sigma_w^2 \frac{1}{D_{l-1}} \sum_{j=1}^{D_{l-1}} \left[\phi\left(\tilde{\mathbf{h}}_j^{l-1,a}\right) \phi\left(\tilde{\mathbf{h}}_j^{l-1,b}\right) \right] + \sigma_b^2, \tag{15}$$

which in the large width limit becomes

$$\tilde{q}_{ab}^{l} = \sigma_{w}^{2} \mathbb{E}_{z_{1}} \left[\mathbb{E}_{z_{2}} \left[\phi(\tilde{u}_{1}) \phi(\tilde{u}_{2}) \right] \right] + \sigma_{b}^{2}$$
(16)

where $\tilde{u}_1 = \sqrt{\tilde{q}_{aa}^{l-1}}z_1$ and $\tilde{u}_2 = \sqrt{\tilde{q}_{bb}^{l-1}}\left[\tilde{c}^{l-1}z_1 + \sqrt{1-(\tilde{c}^{l-1})^2}z_2\right]$, with the correlation between inputs at layer l given by

$$\tilde{c}^l = \tilde{q}_{ab}^l / \sqrt{\tilde{q}_{aa}^l \tilde{q}_{bb}^l}. \tag{17}$$

Here, $z_i \sim \mathcal{N}(0,1)$ for i=1,2 and q_{aa}^l is the variance of $\tilde{\mathbf{h}}_j^{l,a}$.

B Signal propagation in noise regularised ReLU networks

In this section, we give additional details of theoretical results presented in the paper that were specifically derived for noisy ReLU networks.

B.1 Variance of input signals

Let $f(z) = \frac{e^{-z^2/2}}{\sqrt{2\pi}}$, then the variance map in (13) using ReLU, *i.e.* $\phi(a) = \max(0, a)$, becomes

$$\tilde{q}^{l} = \sigma_{w}^{2} \left[\int_{-\infty}^{\infty} f(z)\phi \left(\sqrt{\tilde{q}^{l-1}}z \right)^{2} dz \right] \odot \mu_{2} + \sigma_{b}^{2}
= \sigma_{w}^{2} \left[\int_{-\infty}^{0} f(z)\phi \left(\sqrt{\tilde{q}^{l-1}}z \right)^{2} dz + \int_{0}^{\infty} f(z)\phi \left(\sqrt{\tilde{q}^{l-1}}z \right)^{2} dz \right] \odot \mu_{2} + \sigma_{b}^{2}
= \sigma_{w}^{2} \left[\tilde{q}^{l-1} \int_{0}^{\infty} f(z)z^{2}dz \right] \odot \mu_{2} + \sigma_{b}^{2}
= \sigma_{w}^{2} \left[\frac{\tilde{q}^{l-1}}{2} \odot \mu_{2} \right] + \sigma_{b}^{2}.$$
(18)

B.2 Correlation between input signals

Assuming that the variance map in (18) is at its fixed point \tilde{q}^* , which exits only if $\sigma_w^2 = \frac{2}{\mu_2}$, the correlation map in (16) for a noisy ReLU network is given by

$$\tilde{c}^{l} = \frac{2}{\mu_{2}\tilde{q}^{*}} \int_{-\infty}^{\infty} \int_{-\infty}^{\infty} f(z_{1}) f(z_{2}) \phi(\tilde{u}_{1}) \phi(\tilde{u}_{2}) dz_{2} dz_{1} + \sigma_{b}^{2}$$
(19)

where $\phi(a) = \max(a,0)$, $f(z_i) = \frac{e^{-z_i^2/2}}{\sqrt{2\pi}}$, $\tilde{u}_1 = \sqrt{\tilde{q}^*}z_1$ and $\tilde{u}_2 = \sqrt{\tilde{q}^*}\left[\tilde{c}^{l-1}z_1 + \sqrt{1-(\tilde{c}^{l-1})^2}z_2\right]$. Note that

$$\begin{split} \tilde{u}_1 & \begin{cases} \geq 0, & \text{if } z_1 > 0 \\ < 0, & \text{Otherwise} \end{cases} \\ \tilde{u}_2 & \begin{cases} \geq 0, & \text{if } z_2 > \frac{-\tilde{c}^{l-1}z_1}{\sqrt{1-(\tilde{c}^{l-1})^2}} \\ < 0, & \text{Otherwise} \end{cases} \end{split},$$

therefore (19) becomes

$$\tilde{c}^{l} = \frac{2}{\mu_{2}\tilde{q}^{*}} \int_{0}^{\infty} \int_{\frac{-\tilde{c}^{l-1}z_{1}}{\sqrt{1-(\tilde{c}^{l-1})^{2}}}}^{\infty} f(z_{1})f(z_{2})\tilde{u}_{1}\tilde{u}_{2}dz_{2}dz_{1} + \sigma_{b}^{2}
= \frac{2}{\mu_{2}\tilde{q}^{*}} \sigma_{w}^{2} \int_{0}^{\infty} \int_{\frac{-\tilde{c}^{l-1}z_{1}}{\sqrt{1-(\tilde{c}^{l-1})^{2}}}}^{\infty} f(z_{1})f(z_{2})\sqrt{\tilde{q}^{*}}z_{1}\sqrt{\tilde{q}^{*}} \left[\tilde{c}^{l-1}z_{1} + \sqrt{1-(\tilde{c}^{l-1})^{2}}z_{2}\right] dz_{2}dz_{1} + \sigma_{b}^{2}
= \frac{2\tilde{c}^{l-1}}{\mu_{2}} \int_{0}^{\infty} \int_{\frac{-\tilde{c}^{l-1}z_{1}}{\sqrt{1-(\tilde{c}^{l-1})^{2}}}}^{\infty} f(z_{1})f(z_{2})z_{1}^{2}dz_{2}dz_{1}
+ \frac{2\sqrt{1-(\tilde{c}^{l-1})^{2}}}{\mu_{2}} \int_{0}^{\infty} \int_{\frac{-\tilde{c}^{l-1}z_{1}}{\sqrt{1-(\tilde{c}^{l-1})^{2}}}}^{\infty} f(z_{1})f(z_{2})z_{1}z_{2}dz_{2}dz_{1}. \tag{20}$$

The first term in (20) can then be written as

$$\frac{2\tilde{c}^{l-1}}{\mu_2} \left\{ \int_0^\infty \int_{\frac{-\tilde{c}^{l-1}z_1}{\sqrt{1-(\tilde{c}^{l-1})^2}}}^0 f(z_1)f(z_2)z_1^2 dz_2 dz_1 + \int_0^\infty \int_0^\infty f(z_1)f(z_2)z_1^2 dz_2 dz_1 \right\}. \tag{21}$$

In (21), the first term inside the braces is given by

$$\int_{0}^{\infty} \int_{\frac{-\tilde{c}^{l-1}z_{1}}{\sqrt{1-(\tilde{c}^{l-1})^{2}}}}^{0} f(z_{1})f(z_{2})z_{1}^{2}dz_{2}dz_{1} = \frac{1}{2} \int_{0}^{\infty} f(z_{1})z_{1}^{2} \operatorname{erf}\left(\frac{\tilde{c}^{l-1}z_{1}}{\sqrt{1-(\tilde{c}^{l-1})^{2}}}\right) dz_{1}$$

$$= \frac{1}{2\pi} \left[\tilde{c}^{l-1}\sqrt{1-(\tilde{c}^{l-1})^{2}} + \tan^{-1}\left(\frac{\tilde{c}^{l-1}}{\sqrt{1-(\tilde{c}^{l-1})^{2}}}\right)\right]$$

$$= \frac{1}{2\pi} \left[\tilde{c}^{l-1}\sqrt{1-(\tilde{c}^{l-1})^{2}} + \sin^{-1}\left(\tilde{c}^{l-1}\right)\right] \tag{22}$$

with ${\rm erf}(a)=\frac{1}{\pi}\int_{-a}^a e^{-t^2}dt.$ The second term inside the braces in (21) equals

$$\int_{0}^{\infty} \int_{0}^{\infty} f(z_{1}) f(z_{2}) z_{1}^{2} dz_{2} dz_{1} = \frac{1}{2} \int_{0}^{\infty} f(z_{1}) z_{1}^{2} dz_{1}$$

$$= \frac{1}{4}.$$
(23)

Therfore, (21) becomes

$$\frac{(\tilde{c}^{l-1})^2}{\mu_2 \pi} \sqrt{1 - (\tilde{c}^{l-1})^2} + \frac{\tilde{c}^{l-1}}{\mu_2 \pi} \sin^{-1} \left(\tilde{c}^{l-1} \right) + \frac{\tilde{c}^{l-1}}{2\mu_2} \tag{24}$$

Similarly, the second term in (20) can be split up as follows

$$\frac{2\sqrt{1-(\tilde{c}^{l-1})^2}}{\mu_2} \left\{ \int_0^\infty \int_{\frac{-\tilde{c}^{l-1}z_1}{\sqrt{1-(\tilde{c}^{l-1})^2}}}^0 f(z_1)f(z_2)z_1z_2dz_2dz_1 + \int_0^\infty \int_0^\infty f(z_1)f(z_2)z_1z_2dz_2dz_1 \right\}. \tag{25}$$

The first term inside the braces of (25) is

$$\int_{0}^{\infty} \int_{\frac{-\tilde{c}^{l-1}z_{1}}{\sqrt{1-(\tilde{c}^{l-1})^{2}}}}^{0} f(z_{1})f(z_{2})z_{1}z_{2}dz_{2}dz_{1} = \frac{1}{\sqrt{2\pi}} \int_{0}^{\infty} f(z_{1})z_{1} \left[e^{-\frac{\tilde{c}^{l-1}z_{1}^{2}}{2(1-(\tilde{c}^{l-1})^{2})}} - 1 \right] dz_{1}$$

$$= \frac{1}{\sqrt{2\pi}} \left\{ \frac{1-(\tilde{c}^{l-1})^{2}}{\sqrt{2\pi}} - \frac{1}{\sqrt{2\pi}} \right\}$$

$$= -\frac{(\tilde{c}^{l-1})^{2}}{2\pi}$$
(26)

and the second term is

$$\int_{0}^{\infty} \int_{0}^{\infty} f(z_{1})f(z_{2})z_{1}z_{2}dz_{2}dz_{1} = \frac{1}{\sqrt{2\pi}} \int_{0}^{\infty} f(z_{1})z_{1}dz_{1}$$

$$= \frac{1}{2\pi}.$$
(27)

Putting these two terms together, (25) becomes

$$-\frac{(\tilde{c}^{l-1})^2}{\mu_2 \pi} \sqrt{1 - (\tilde{c}^{l-1})^2} + \frac{1}{\mu_2 \pi} \sqrt{1 - (\tilde{c}^{l-1})^2}.$$
 (28)

Finally, summing all the terms in (24) and (28) gives (19) as

$$\tilde{c}^{l} = \frac{1}{\mu_{2}} \left\{ \frac{\tilde{c}^{l-1} \sin^{-1} \left(\tilde{c}^{l-1} \right) + \sqrt{1 - (\tilde{c}^{l-1})^{2}}}{\pi} + \frac{\tilde{c}^{l-1}}{2} \right\}. \tag{29}$$

We note that for the noiseless case, (29) is identical to the result recently obtained by Hayou et al. (2018), where the authors used a slightly different approach.

B.3 Depth scales for trainability

We recap the result in Schoenholz et al. (2017) and adapt the derivation for the specific case of a noisy ReLU network. Let $c^l = c^* + \varepsilon^l$, such that as long as $\lim_{l\to\infty} c^l = c^*$ exist we have that $\varepsilon\to 0$ as $l\to\infty$. Then Schoenholz et al. (2017) derived the following asymptotic recurrence relation

$$\varepsilon^{l+1} = \varepsilon^l \chi(c^*) + \mathcal{O}((\varepsilon^l)^2), \tag{30}$$

where

$$\chi(c^*) = \sigma_w^2 \mathbb{E}_{z_1} \left[\mathbb{E}_{z_2} \left[\phi'(\tilde{u}_1^*) \phi'(\tilde{u}_2^*) \right] \right], \tag{31}$$

with $\tilde{u}_1^* = \tilde{u}_1 = \sqrt{\tilde{q}^*}z_1$ and $\tilde{u}_2^* = \sqrt{\tilde{q}^*}\left[\tilde{c}^*z_1 + \sqrt{1-(\tilde{c}^*)^2}z_2\right]$. Now, specifically for a noisy ReLU network where $\sigma_w^2 = \frac{2}{\mu_2}$, we have that

$$\chi(c^*) = \frac{2}{\mu_2} \int_{-\infty}^{\infty} \int_{-\infty}^{\infty} f(z_1) f(z_2) \phi'(\tilde{u}_1^*) \phi'(\tilde{u}_2^*) dz_2 dz_1
= \frac{2}{\mu_2} \int_{0}^{\infty} \int_{-\frac{c^* z_1}{\sqrt{1 - (c^*)^2}}}^{\infty} f(z_1) f(z_2) dz_2 dz_1
= \frac{2}{\mu_2} \int_{0}^{\infty} f(z_1) \frac{1}{2} \left[\text{erf} \left(\frac{c^* z_1}{\sqrt{2} \sqrt{1 - (c^*)^2}} \right) + 1 \right] dz_1
= \frac{2}{\mu_2} \left[\frac{1}{2\pi} \tan^{-1} \left(\frac{c^*}{\sqrt{1 - (c^*)^2}} \right) + \frac{1}{4} \right]
= \frac{1}{\mu_2 \pi} \left[\sin^{-1} (c^*) + \frac{\pi}{2} \right]$$
(32)

Note that $\chi(c^*)$ is a constant, thus for large l the solution to the recurrence relation in (30) is expected to be exponential, i.e. $\varepsilon^l \sim e^{-l/\xi_c}$. Here ξ_c , is considered the depth scale, which controls how deep discriminatory information about the inputs can propagate through the network. We can then solve for ξ_c to find

$$\xi_c = -1/\ln(\chi(c^*)) = -\ln\left[\frac{\sin^{-1}(c^*)}{\mu_2 \pi} + \frac{1}{2\mu_2}\right]^{-1}.$$
 (33)

B.4 Variance of error signals

Under the mean field assumption, Schoenholz et al. (2017) approximates the error signal at layer l by a zero mean Gaussian with variance

$$\tilde{q}_{\delta}^{l} = \tilde{q}_{\delta}^{l+1} \frac{D_{l+1}}{D_{l}} \sigma_{w}^{2} \mathbb{E}_{z} \left[\phi' \left(\sqrt{\tilde{q}^{l}} z \right)^{2} \right], \tag{34}$$

where $\tilde{q}_{\delta}^l = \mathbb{E}[(\tilde{\delta}_i^l)^2]$, with $\tilde{\delta}_i^l = \phi'(\tilde{\mathbf{h}}_i^l) \sum_{j=1}^{D_{l+1}} \tilde{\delta}_j^{l+1} W_{ji}^{l+1}$. In our context, for a critically initialised noisy ReLU network we have that

$$\tilde{q}_{\delta}^{l} = \tilde{q}_{\delta}^{l+1} \frac{D_{l+1}}{D_{l}} \frac{2}{\mu_{2}} \int_{0}^{\infty} f(z)dz$$

$$(35)$$

$$=\tilde{q}_{\delta}^{l+1} \frac{D_{l+1}}{D_l} \frac{1}{\mu_2}.$$
 (36)

B.5 Correlation between error signals

The covariance between error signals is approximated using

$$\tilde{q}_{ab,\delta}^{l} = \tilde{q}_{ab,\delta}^{l+1} \frac{D_{l+1}}{D_{l+2}} \sigma_w^2 \mathbb{E}_{z_1} \left[\mathbb{E}_{z_2} \left[\phi'(\tilde{u}_1) \phi'(\tilde{u}_2) \right] \right], \tag{37}$$

where \tilde{u}_1 and \tilde{u}_2 are defined as was done in the forward pass. Here, we simply use the result in (32) for noisy ReLU networks to find

$$\tilde{q}_{ab,\delta}^{l} = \tilde{q}_{ab,\delta}^{l+1} \frac{D_{l+1}}{D_{l+2}} \chi(c^*)$$
(38)

$$= \tilde{q}_{ab,\delta}^{l+1} \frac{D_{l+1} \left[\sin^{-1} \left(c^* \right) + \frac{\pi}{2} \right]}{D_{l+2} \mu_2 \pi}.$$
 (39)

C Experimental details

In this section we provide additional details regarding our experiments in the paper. Code to reproduce all the experiments is available at https://github.com/ElanVB/noisy_signal_prop.

C.1 Input data

For all experiments the network input data properties that remain consistent (unless stated otherwise) are as follows: each observation consists of 1000 features and each feature value is drawn i.i.d. from a standard normal distribution.

C.2 Variance propagation dynamics

The experiments conducted to gather results for Figures 2 and 3 aim to empirically show the relationship between the variances at arbitrary layers in a neural network.

Iterative map: For the results depicted in Figures 2 (a) and 3 (a), the experimental set up is as follows. The data used as input to these experiments comprises of 30 sets of 30 observations. The input is scaled such that the variance of observations within each set is the same and the variance across each set is different and forms a range of $q_{\text{set}} \in [0, 15]$. As such, our results are averaged over 30 observations and 50 samplings of initial weights to a single hidden-layer network.

Convergence dynamics: For the results depicted in Figures 2 (b) and 3 (b), the experimental set up is as follows. The data used as input to these experiments comprises of a set of 50 observations scaled such that each observation's variance is four (q=4). As such, our results are averaged over 50 observations and 50 samplings of initial weights to a 15 hidden-layer network.

C.3 Correlation propagation dynamics

The experiments conducted to gather results for Figure 4 and 5 aim to empirically show the relationship between the correlations of observations at arbitrary layers in a neural network.

Iterative map: For the results depicted in Figure 4 (a), the experimental set up is as follows. The data used as input to these experiments comprises of 50 sets of 50 observations. The first observation in each set is sampled from a standard normal distribution and subsequent observations are generated such that the correlation between the first element and the i^{th} element form a range of $\text{corr}_{0,i} \in [0,1]$. As such, our results are averaged over 50 observations and 50 samplings of initial weights to a single hidden-layer network.

Convergence dynamics: For the results depicted in Figure 4 (b), the experimental set up is as follows. The data used as input to these experiments comprises of three sets of 50 equally correlated observations. Each set has a different correlation value such that $corr_{set} \in \{0, 0.5, 0.9\}$. As such, our results are averaged over 50 observations and 50 samplings of initial weights to a 15 hidden-layer network.

Confirmation of exponential rate of convergence for correlations: This section discusses how the results depicted in Figure 5 are acquired. These experiments support the assumption that the rate of convergence for correlations is exponential when using noise regularisation with rectifier neural networks. The experimental set up for this section is very similar to that of the above convergence dynamics experiment, the only difference being the statistics we calculate from the correlation values. The aspect of this experiment that may seem the most unclear is the reason why we claim that the negative inverse slope of a linear fit to the log differences in correlation should match the theoretical values for ξ_c . The derivation to justify this is as follows. If a good fit of the form al + b can be found in the logarithmic domain for the rate of convergence, it would strongly indicate that the convergence rate is exponential. Following this, we set the problem up like so:

$$|c^{l} - c^{*}| \approx e^{-l/\xi_{c}}$$
$$\therefore \ln\left(|c^{l} - c^{*}|\right) \approx \frac{-l}{\xi_{c}}.$$

Let us now assume that $\ln (|c^l - c^*|)$ can be linearly approximated:

$$\therefore \ln (|c^{l} - c^{*}|) \approx al + b,$$

$$\therefore al + b \approx \frac{-l}{\xi_{c}},$$

$$\therefore \xi_{c} \approx \frac{-l}{al + b}.$$

Since we are concerned with deep neural networks, we can take the limit as l becomes arbitrarily large and see that as l grows the effect of b decreases $(\lim_{l\to\infty} |al| \gg |b|)$. Thus, we continue like so:

$$\lim_{l \to \infty} \xi_c \approx \lim_{l \to \infty} \frac{-l}{al}$$
$$\approx -\frac{1}{a}.$$

Thus, we have come to the finding that if the correlation rate of convergence is exponential and we work with deep neural networks, the negative inverse slope of a linear fit to the log differences in correlation should match the theoretical values for ξ_c . Figure 5 shows that the theory closely matches this approximation.

C.4 Depth scales

This section handles the experiments conducted related to determining the maximum depth variance information can stably propagate through a network and the depth at which these networks can be trained, both depicted in Figure 6.

The MNIST and CIFAR-10 datasets were used and were pre-processed using standard techniques. Throughout these experiments mini-batches of 128 observations were used.

Variance depth scales: The experiments depicted in Figures 6 (a) and (d) are interested in testing the numerical stability of networks initialised using different σ_w^2 values while using 32-bit floating point

numbers. To test the depth of stable variance propagation, a network with 1000 hidden layers is used. The network used in this experiment makes use of dropout with p=0.6, where p is the probability of keeping a neuron's value, thus the critical value for σ_w^2 is 1.2. As such, a linearly spaced range of $\sigma_w^2 \in [0.1, 2.5]$ is used to select 25 different values.

We use the following approach to predict the depth beyond which variances become numerically unstable. At criticality for multiplicative noise $(\sigma_w, \sigma_b) = (\sqrt{2/\mu_2}, 0)$, however, for weights initialised off this critical point (18) becomes

$$\tilde{q}^{l} = \tilde{q}^{l-1} \left(\frac{\sigma_{w}^{2} \mu_{2}}{2} \right)
= \left[\tilde{q}^{l-2} \left(\frac{\sigma_{w}^{2} \mu_{2}}{2} \right) \right] \left(\frac{\sigma_{w}^{2} \mu_{2}}{2} \right)
= \tilde{q}^{0} \left(\frac{\sigma_{w}^{2} \mu_{2}}{2} \right)^{l}.$$
(40)

If $\sigma_w^2>\frac{2}{\mu_2}$, we let $\tilde{q}^l=K$, where K is the largest positive number representable by the computer. In our case, using 32-bit floating point precision, this number is equal to 3.4028235×10^{38} . Otherwise, if $\sigma_w^2<\frac{2}{\mu_2}$ we select $K=1.1754944\times 10^{-38}$, the smallest possible positive number. Furthermore, let L^* represent the layer l in (40) at which the value K is reached, then we can scale our input data such that $\tilde{q}^0=1$ and solve for L^* to find

$$L^* = \ln(K) / \ln\left(\frac{\sigma_w^2 \mu_2}{2}\right). \tag{41}$$

Therefore, we expect numerical instability issues to occur beyond a depth of L^* .

Trainable depth scales: The experiments depicted in Figures 6 (b), (c), (e) and (f) are concerned with determining at what depth a critically initialised network with a specified dropout rate can train effectively. To this end, 10 linearly spaced values for dropout on the range $p \in [0.1, 1.0]$ and 10 linearly spaced network depths on the integer range $l \in [2, 40]$ are tested.

The task presented to the network in this experiment is to learn the identity function within 200 epochs. As such, the network is set up as an auto-encoder and uses stochastic gradient decent with a learning rate of 10^{-3} . The input data is divided into a training and validation set, each containing 50000 and 10000 observations respectively.

C.5 Additional results

In this section we provide some additional experiments on the training dynamics of deep noisy ReLU networks from different initialisations.

In Figure 7 we compare the standard "He" initialisation (blue) with the critical initialisation (green) for a ReLU network with dropout regularisation (p=0.8). By not initialising at criticality due to dropout noise, the variance map for the "He" strategy no longer lies on the identity line in (a) and as a result, the forward propagating signal can be seen to explode in (b). However, by compensating for the amount of injected noise, the above derived critical initialisation for dropout preserves the signal throughout the entire forward pass, with roughly constant variance dynamics.

Next, we provide some additional experiments on the trainability of deep ReLU networks with dropout on real-world data sets.

From our analysis in the paper, we expect that as the depth of the network increases, any initialisation strategy that does not factor in the effects of noise, will cause the forward propagating signal to become increasingly unstable. For very deep networks, this might cause the signal to either explode or vanish, even within the first forward pass, making the network untrainable.

To test this, we trained a denoising autoencoder network with dropout noise (p=0.6) on MNIST and CIFAR-10 using squared reconstruction loss. We consider several network depths (L=30,100,200), learning rates $(\alpha=0.1,0.01,0.001,0.0001)$ and optimisation procedures (SGD and Adam), with 1000 neurons in each layer. The results for training on CIFAR-10 are shown in Figure 8 for both the "He" intialisation (blue) and the critical dropout initialisation (green). (For MNIST, see Figure 9; the

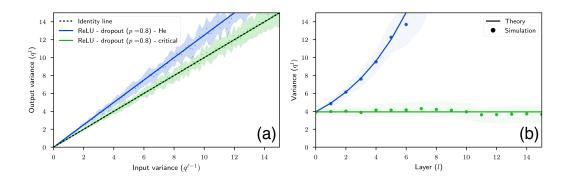


Figure 7: Critical initialisation for ReLU networks with dropout. Lines correspond to theoretical predictions and points to numerical simulations, for random ReLU networks with dropout (p=0.8), initialised according to the method proposed by He et al. (2015) (blue) and at criticality (green). (a): Iterative variance map where the identity line is displayed as a dashed black line. (b): Variance dynamics during forward signal propagation.

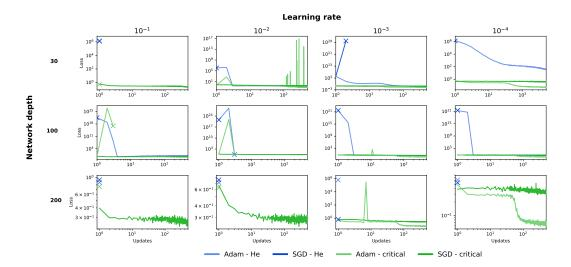


Figure 8: Comparing the "He" initialisation strategy to critical dropout initialisation for ReLU networks using dropout (p=0.6) on CIFAR-10. While networks initialised at criticality (green) are able to train at large depths (L=200) as seen in the bottom row, networks initialised with the "He" strategy (blue) become untrainable irrespective of the chosen learning rate or optimisation procedure. An "X" marks the point at which a network completely stopped training. Training losses and number of network updates are shown in log-scale.

core trends and resulting conclusions regarding network trainability is the same for both data sets, which we discuss below.)

As the depth increases, moving from the top to the bottom row in Figure 8, networks initialised at the critical point for dropout seem to remain trainable even up to a depth of 200 layers (we see the loss start to decrease over five epochs). In contrast, networks using the "He" initialisation become increasingly more difficult to train, with no training taking place at very large depths. These findings make sense in terms of the variance dynamics analysed in the paper, however, these experimental successes seem to run counter to our theoretical analysis of trainable depth scales (this contradiction can also be seen in Figure 6). Understanding this discrepancy is of particular interest to us.

To verify that the lack of training in Figure 8 is due to poor signal propagation, we plot the empirical variance of the pre-activations in Figure 10, for the first forward pass of a 200 layer autoencoder

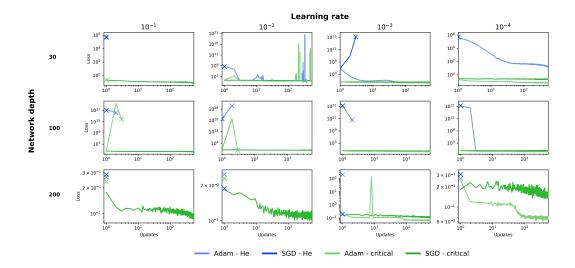


Figure 9: Comparing the "He" initialisation strategy to critical dropout initialisation for ReLU networks using dropout (p=0.6) on MNIST. While networks initialised at criticality (green) are able to train at large depths (L=200) as seen in the bottom row, networks initialised with the "He" strategy (blue) become untrainable irrespective of the chosen learning rate or optimisation procedure. An "X" marks the point at which a network completely stopped training. Training losses and number of network updates are shown in log-scale.

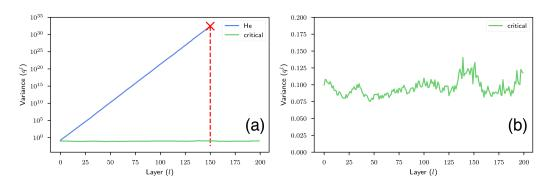


Figure 10: Variance dynamics for signal propagation in the first forward pass for a 200 layer autoencoder network fed a batch of 500 training examples from CIFAR-10. (a) Exploding activation variance (blue) reaching overflow levels (marked with a red "X") for the "He" intialisation, with no signal reaching the output layer (shown in log-scale). (b) Zoomed in display of the roughly constant variance dynamics in (a) for the critical dropout initialisation.

network. For the "He" initialisation, the variance in (a) grows rapidly to the point of causing numerical instability and overflow (indicated by the red dashed line), well before any signal is able to reach the output layer. However as shown in (b), by initialising at criticality, signal is able to propagate reliably even at large depths.

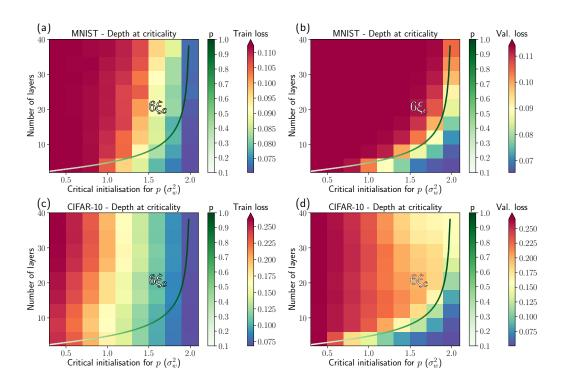


Figure 11: Depth scale experiments on MNIST and CIFAR-10. (a) Depth scales fit to the training loss on MNIST for networks initialised at criticality for dropout rates p=0.1 (severe dropout) to p=1 (no dropout). (b) Depth scales fit to the validation loss on MNIST. (c) - (d): Similar to (a) - (c), but for CIFAR-10.